JACC: CARDIOVASCULAR IMAGING VOL. 5, NO. 3, 2012

ISSN 1936-878X/$36.00
PUBLISHED BY ELSEVIER INC. DOI:10.1016/j.jcmg.2011.11.013

Relation of Torsion and Myocardial Strains to LV Ejection Fraction in Hypertension

Mustafa I. Ahmed, MD,* Ravi V. Desai, MD,* Krishna K. Gaddam, MD,*
Bharath A. Venkatesh, PhD,§ Shilpi Agarwal, MS, MD,* Seidu Inusah, MS,†
Steven G. Lloyd, MD, PhD,*‡ Thomas S. Denney Jr, PhD,§ David Calhoun, MD,*
Louis J. Dell'italia, MD,*‡ Himanshu Gupta, MD*‡

Birmingham and Auburn, Alabama

OBJECTIVES The goal of this study was to define the mechanism of preserved ejection fraction (EF) despite depressed myocardial strains in hypertension (HTN).

BACKGROUND Concentric left ventricular (LV) remodeling in HTN may have normal or supranormal EF despite depressed myocardial strains. The reason for such discordance is not clear. The aim of this study was to comprehensively evaluate the LV mechanics in a well-defined HTN population to define underlying reasons for such a paradox.

METHODS Sixty-seven patients with resistant HTN and 45 healthy control subjects were studied by cardiac magnetic resonance imaging and tissue tagging with 3-dimensional analysis. Amplitude and directional vector of longitudinal (Ell), circumferential (Ecc), and principal strain for maximal shortening (E3) were computed at basal, mid, and distal LV levels, respectively. LV torsion, defined as the rotation angle of apex relative to base, and LV twist, which accounts for the effects of differential LV remodeling on torsion for comparison among the 2 groups, were also calculated.

RESULTS LV mass index and LV mass/LV end-diastolic volume ratio were significantly higher in the HTN group compared with controls, consistent with concentric LV remodeling. Ell and Ecc were significantly decreased in amplitude with altered directional vector in HTN compared with controls. However, the amplitude of E3 was similar in the 2 groups. Torsion and twist were significantly higher in HTN, which was mainly due to increase in apical rotation. The HTN group demonstrated significantly increased LV wall thickening compared with controls that resulted in greater LVEF in the HTN group compared with controls (70% vs. 65%, $p < 0.001$, respectively).

CONCLUSIONS In compensated LV remodeling secondary to HTN, there is increased LV wall thickening with preserved E3 and increased torsion compared with normal controls. This, therefore, contributes to supranormal LVEF in HTN despite depressed longitudinal and circumferential strains. (J Am Coll Cardiol Img 2012;5:273–81) © 2012 by the American College of Cardiology Foundation

From the *Division of Cardiovascular Medicine, Department of Medicine, University of Alabama at Birmingham, Birmingham, Alabama; †Department of Biostatistics, University of Alabama at Birmingham, Birmingham, Alabama; ‡Birmingham Veteran Affairs Medical Center, Birmingham, Alabama; and the §Department of Electrical and Computer Engineering, Auburn University, Auburn, Alabama. Funded by National Institutes of Health grants NIH P50-HL077100 (L.J.D.) and NIH R01-HL104018 (H.G.). The authors have reported that they have no relationships relevant to the contents of this paper to disclose.

Manuscript received January 20, 2011; revised manuscript received November 7, 2011, accepted November 10, 2011.

Hypertension (HTN) is the leading risk factor for the development of heart failure (1). In response to the increased afterload of arterial HTN, the left ventricle (LV) undergoes concentric LV remodeling, which normalizes LV wall stress and maintains LV ejection fraction (EF) in a normal or even supernormal range (2). Previous studies have shown that LV midwall shortening by echo and LV strains by magnetic resonance tagging are impaired in patients with hypertensive LV remodeling, suggesting cardiomyocyte dysfunction despite normal LVEF (3–5). In usual circumstances, LV deformation as assessed by measurement of myocardial strains is directly correlated with LVEF. However, in HTN with preserved EF, there appears to be discordance between measurement of regional myocardial strains and global EF. The reason for such discordance is unclear.

See page 282

ABBREVIATIONS AND ACRONYMS

BMI = body mass index

CMR = cardiac magnetic resonance

ECG = electrocardiographically

EF = ejection fraction

HTN = hypertension

LV = left ventricular/ventricle

LV systolic torsion is an important mechanism of wall thickening and a primary component of normal systolic function (6–10). Some have also proposed an important role of transverse shear in the observed wall thickening (11). Torsion represents the myocardial rotation gradient from the base to apex of the LV. It acts to normalize LV wall stress by minimizing transmural gradients of fiber strain and thereby increase energy efficiency by reducing oxygen demand (7,12,13). Cardiac magnetic resonance (CMR) tissue tagging techniques allow accurate noninvasive assessment of 3-dimensional (3D) LV remodeling, myocardial strains, and torsion (14–17). The aims of the current study were 2-fold: 1) to comprehensively define regional and global cardiac mechanics and remodeling parameters using 3D CMR with myocardial tagging in a well-characterized HTN patient population; and 2) to define the mechanism of preserved EF despite altered myocardial strains in such a patient population.

METHODS

Study patients. This study prospectively evaluated consecutive patients referred for specialist evaluation of resistant HTN. Control group comprised volunteers who were healthy with no history of cardiovascular disease and not using any prescription medication. Resistant HTN was defined as uncontrolled HTN (>140/90 mm Hg) determined at 2 or more clinic visits despite the use of 3 or more antihypertensive medications at optimal doses. Patients with coronary artery disease or diabetes were also excluded from the study. Subjects with a history of congestive heart failure, chronic kidney disease (creatinine clearance <60 ml/min), or chronic steroid therapy were excluded from study participation. Secondary causes of hypertension other than hyperaldosteronism, such as renovascular HTN, pheochromocytoma, or Cushing's syndrome, were excluded as clinically indicated. The HTN group consisted of 67 subjects and the control group 45 subjects. The study protocol was approved by our institutional review board, and informed consent was obtained from all participants.

Magnetic resonance imaging. Magnetic resonance imaging was performed on a 1.5-T magnetic resonance scanner (GE Signa, Milwaukee, Wisconsin) optimized for cardiac application. Electrocardiographically (ECG)-gated breath-hold steady-state free-precision technique was used to obtain standard 2-, 3-, and 4-chamber and short-axis views with following general parameters: prospective ECG gating, slice thickness = 8 mm, zero interslice gap, field of view = 40 × 40 cm, scan matrix = 256 × 128, flip angle = 45°, repetition/echo times = 3.8/1.6 ms. Twenty cardiac phases were reconstructed with 8 to 10 views per segment. Short-axis stack was positioned from an end-diastolic 4-chamber image, centered parallel to the mitral annulus and perpendicular to the septum, starting 1 cm proximal to the mitral valve to 1 cm beyond the apex.

Tagged CMR was done on exact slice prescriptions as in the previous text by applying grid tagging to the short-axis views and stripe tagging to long-axis views using spatial modulation of magnetization encoding gradients method (FGR-SPAMM) as previously described (18) with the following general parameters: prospective ECG gating, slice thickness = 8 mm, zero interslice gap, field of view = 40 × 40 cm, scan matrix = 256 × 128, flip angle = 10°, repetition/echo times = 8.0/4.2 ms, views per segment = 8 to 10, tag spacing = 7 mm, number of reconstructed cardiac phases = 20 (Fig. 1).

Geometric analysis. The 3D LV geometric parameters were measured from endocardial and epicardial contours manually traced on cine images acquired near end-diastole and end-systole. The contours were traced to exclude the papillary muscles. The contour data were then transformed to a coordinate system aligned along the long axis of the LV and converted to a prolate spheroidal coordinate system

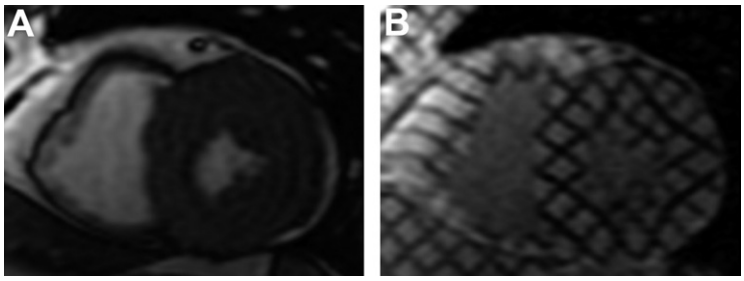

Figure 1. Short-Axis Images of the LV Comparing the Cine SSFP Technique With the FGR-SPAMM Method

Representative example of a short-axis image of the left ventricle (LV) **(left)** using cine steady-state free-precession (SSFP) technique and the corresponding tagged image **(right)** obtained using spatial modulation of magnetization encoding gradients (FGR-SPAMM) method.

as described (19). The prolate spheroidal coordinate system has 1 radial coordinate (λ) and 2 angular coordinates (μ,θ), and was used because surfaces of constant λ are ellipsoids, which more closely approximate the shape of the LV wall than cylinders or spheres. Cubic B-spline surfaces with 12 control points in the circumferential (θ) direction and 10 control points in the longitudinal direction (μ) were fit to the λ coordinates of the endocardial and epicardial contours for each time frame. The fit used the smoothing term described (19) with $\alpha = 0$, $\beta = 0$, $\gamma = 0.1$.

The 3D surface curvatures were computed using standard formulas (20) at the standard wall segments (excluding the apex) (21). Myocardial mass was calculated by multiplying end-diastolic myocardial muscle volume by 1.05 g/cm^3. The 3D wall thickness was computed at the same segments by measuring the distance from a point on the epicardial surface to the closest point on the epicardial surface along a line perpendicular to the epicardial surface. The radius of curvature to wall thickness ratio (R/T), was computed by computing the reciprocal of the product of the endocardial circumferential curvature (κ) and wall thickness (h). End-systolic wall stress was computed according to the formula (2):

$$\text{LVES Wall Stress} = 0.133\frac{P}{2\kappa h\left(1+\frac{\kappa h}{2}\right)}$$

where P is the end-systolic LV blood pressure measured by a cuff measurement at the time of the CMR scan. The apex curvatures and apex curvature index (22) were computed from endocardial contours drawn on 2- and 4-chamber view images at end-diastole and end-systole. The apex curvatures index was defined as the average of LV apex radius of curvature calculated from 2- and 4-chamber views divided by the LV inner radius. The sphericity index was defined as the ratio of LV long-axis length to LV inner diameter. The LV long-axis length was computed from LV endocardial contours drawn on a 4-chamber view.

Strain analysis. The 3D LV strain was measured from tagged images at end-systole, which was defined by visual inspection of the image data as the time frame with maximum contraction. Tag lines were tracked with the algorithm described in Denney et al. (23) and edited, if necessary, by an expert user. The 3D deformation and Lagrangian strain

Table 1. Baseline Characteristics

	HTN (n = 67)	Control (n = 45)	p Value
Age, yrs	55 (12.4)	41 (12.6)	<0.001
Age range, yrs	26–76	20–69	
Females	46.3	53.3	NS
Caucasians	55.2	67.4	NS
SBP, mm Hg	144 (16)	118 (13)	<0.001
DBP, mm Hg	88 (12)	74 (11)	<0.001
HR, beats/min	68 (12)	72 (12)	0.047
Duration of HTN, yrs	16.7 (10)	0	
Number of anti-HTN medications	4 (1)	0	
Beta-blocker %	76.11	0	
ACE-I	64.17	0	
ARB	53.73	0	
CCB	68.65	0	
Diuretic	92.53	0	
Other	40.29	0	
BUN, mg/dl	13.8 (6)	11.9 (3.7)	NS
Creatinine, mg/dl	1 (0.3)	1 (0.2)	NS
Weight, lbs	208.4 (45.7)	173.9 (43.1)	<0.001
BMI, kg/m^2	31.9 (5.8)	26.3 (6)	<0.001
BSA, m^2	2.03 (0.27)	1.92 (0.24)	0.024

Values are % or mean ± SD. Significant p value <0.05.
ACE-I = angiotensin-converting enzyme inhibitor; ARB = angiotensin receptor blocker; BMI = body mass index; BSA = body surface area; BUN = blood urea nitrogen; CCB = calcium channel blocker; DBP = diastolic blood pressure; HR = heart rate; HTN = hypertension; NS = not significant; SBP = systolic blood pressure.

was computed by fitting a B-spline deformation model in prolate spheroidal coordinates to the tag line data (24). Normal strains were computed in the radial, circumferential, and longitudinal directions. Principal strains and associated principal directions were also computed. The first principal strain (E1) was approximately aligned in the radial direction and is the maximum thickening strain. The second and third principal strains (E2 and E3) were approximately aligned with the longitudinal and circumferential directions respectively. The third principal strain (E3) is the maximum contraction strain.

The 3D LVES torsion angle was defined as the LVES rotation angle, φ, of the apex relative to the base. The 3D LVES twist, T, was computed from the rotation angle by the following formula (25,26):

$$T = \frac{(\varphi_{apex} - \varphi_{base}) \times (\rho_{apex} - \rho_{base})}{2L}$$

where ρ is the epicardial radius and L is the distance between the basal and apical slices.

All strains were computed at the midwall of all segments in the American Heart Association 17-segment model (21) except the apex (segment 17). For purposes of data analysis, the LV was divided into 3 levels: base, mid, and distal. The strain parameters at each individual level were obtained by averaging the ventricular segments encompassing the whole ventricular wall at that level (6 segments at the base and mid levels, 4 segments at the distal level).

Statistical analysis. Continuous variables are reported in terms of means and standard deviations of means. Comparison was performed using unpaired t test. Normality of distribution was tested using Kolmogorov-Smirnov test. For variables that were not normally distributed, Mann-Whitney test was also performed. Since the results were similar, these data are not reported except for variables where the tests showed some difference, and then Mann-Whitney values are reported. The Fisher exact test was used for categorical variables. For all measurements, the level of significance was defined as p value <0.05. To minimize the inflation of the probability of a type 1 error due to multiple testing, Bonferroni adjustment was done whereby we divided the level of significance by the number of tests. We also created multivariate model for torsional and strain parameters to adjust for age and body mass index (BMI) using linear regression models.

RESULTS

Patient demographics. Baseline patient characteristics for control subjects and HTN, including details of antihypertensive therapy, are outlined in Table 1. As expected, systolic and diastolic blood pressures were significantly higher in the HTN group despite taking an average of 4.15 antihypertensive medications. There were no significant differences in gender or race between the 2 groups. However, the HTN group was more obese, as reflected by body weight and BMI measurements.

MRI-derived indexes of LV geometry and torsion. Global parameters for assessment of LV geometry for control subjects and the HTN group are outlined in Table 2. The HTN group had significantly higher EF as compared with controls. There were no significant differences in LV end-diastolic volume and end-systolic volume between controls versus HTN. At end-diastole, LV in the HTN group compared with controls demonstrated a lower sphericity index and higher apical curvature index. Torsional measurements indicated that both peak torsion and twist measured at end-systole were significantly higher in the HTN group as compared with controls. Torsion and twist remained significantly higher despite adjusting for age alone (β coefficient: 3.19, p = 0.002, and β coefficient: 1.39,

Table 2. LV Geometry and Torsion

	HTN (±SD)	Control (±SD)	p Value
LVEDD, cm	5.12 (0.58)	5.01 (0.46)	NS
LVESD, cm	3.42 (0.62)	3.52 (0.40)	NS
LVEDV, ml	139.3 (42.7)	128.9 (26.5)	NS
LVESV, ml	43.1 (20.7)	45.3 (12.7)	NS
LVED sphericity index	1.66 (0.22)	1.78 (0.18)	0.002
LVES sphericity index	1.97 (0.39)	1.97 (0.26)	NS
LVED apex curvature, cm^{-1}	1.38 (0.37)	1.50 (0.32)	0.049
LVES apex curvature, cm^{-1}	3.84 (2.41)	3.12 (1.07)	NS
LVED apex curvature index	0.32 (0.08)	0.28 (0.06)	0.009
LVES apex curvature index	0.21 (0.1)	0.21 (0.07)	NS
LV mass, g	132.88 (41.58)	95.67 (25.56)	<0.001
LV mass index 1, mass/BSA	63.89 (17.59)	49.69 (10.76)	<0.001
LV mass index 2, mass/$Ht^{2.7}$	30.24 (8.20)	21.68 (5.06)	<0.001
Mass/LVEDV, gm/ml	0.98 (0.25)	0.75 (0.17)	<0.001
LVEF, %	70 (8.3)	65 (5.5)	<0.001
LVES torsion angle,°	18.16 (4.50)	14.05 (3.02)	<0.001
LVES twist,°	6.31 (1.51)	4.56 (0.95)	<0.001
LVES rotation, distal,°	14.42 (3.95)	9.73 (3.56)	<0.001

Significant p value <0.05.
ED = end-diastolic; ES = end-systolic; Ht = height; LV = left ventricular; LVED = left ventricular end-diastolic; LVEDD = left ventricular end-diastolic diameter; LVEDV = left ventricular end-diastolic volume; LVEF = left ventricular ejection fraction; LVES = left ventricular end-systolic; LVESD = left ventricular end-systolic diameter; other abbreviations as in Table 1.

$p < 0.001$, respectively) or age and BMI together (β coefficient: 3.60, $p < 0.001$, and β coefficient: 1.62, $p < 0.001$, respectively). Furthermore, the effect on overall LV torsion and twist was predominantly due to distal LV segment rotation that was higher in HTN compared with controls. On subgroup analysis based on the gender (Tables 3 and 4), the differences in torsion and twist persisted in the HTN group compared with controls.

MRI-derived indexes of regional LV remodeling and wall stress. Regional changes in LV shape and wall stress are described in Table 5. There were no differences in the end-diastolic circumferential and longitudinal curvatures at various LV levels. LV wall thickness and thickening were higher in the HTN group as compared with controls at all levels and during both systole and diastole. Similarly, the LV demonstrated concentric remodeling in the HTN group as compared with controls during both systole and diastole as measured by R/T ratio. LV wall thickening was increased in the HTN group compared with controls. Furthermore, there was reduction in LV wall stress in the HTN group as compared with controls at end-systole. These changes, therefore, indicate that the HTN group had compensated LV remodeling with higher EF as compared with controls.

MRI-derived regional LV strain magnitude and directionality. We calculated E3 (which is the principal strain in the direction of maximal shortening) and also longitudinal (Ell) and circumferential (Ecc) strains (these strain measurements are oriented with respect to the long axis of the LV) at all 3 levels (Table 6). We found significant reduction in Ecc at mid and distal LV segments in HTN. Ell was also reduced at the basal and mid LV segment in the HTN group compared with controls. Results remained similar for Ecc when adjusted for age (β coefficient: -1.82, $p = 0.003$) or age and BMI together (β coefficient: -1.63, $p = 0.02$). Results for Ell also remained similar when adjusted for age (β coefficient: -2.07, $p = 0.003$). However, the results were not statistically significant for Ell when adjusted for both age and BMI together (β coefficient: -1.43, $p = 0.06$). E3, that is, the maximal shortening, was almost identical between the 2 groups at all 3 levels, indicating that there may be changes in the directionality of strain tensors. Indeed, when we measured the directionality of the principal strain tensors, we found they were significantly less circumferential in the HTN group relative to the normal group as described in Table 7 and Figure 2.

Table 3. LV Geometry and Torsion (Male)

	HTN (±SD)	Control (±SD)	p Value
LVEDD, cm	5.28 (0.64)	5.21 (0.39)	NS
LVESD, cm	3.64 (0.59)	3.60 (0.38)	NS
LVEDV, ml	160.2 (49.7)	138.9 (25.3)	0.078
LVESV, ml	53.3 (21.1)	47.9 (12.1)	NS
LVED sphericity index	1.70 (0.20)	1.78 (0.16)	NS
LVES sphericity index	1.97 (0.42)	2.00 (0.27)	NS
LVED apex curvature, cm^{-1}	1.39 (0.43)	1.52 (0.38)	NS
LVES apex curvature, cm^{-1}	3.65 (2.43)	3.18 (0.96)	NS
LVED apex curvature index	0.32 (0.08)	0.28 (0.06)	0.057
LVES apex curvature index	0.21 (0.11)	0.19 (0.06)	NS
LV mass, g	157.62 (36.34)	110.88 (24.06)	<0.001
LV mass index 1, mass/BSA	68.73 (18.42)	53.97 (9.81)	0.002
LV mass index 2, mass/$Ht^{2.7}$	29.74 (7.82)	23.02 (5.08)	<0.001
Mass/LVEDV, gm/ml	1.02 (0.24)	0.81 (0.17)	0.001
LVEF, %	67 (6.8)	66 (4.5)	NS
LVES torsion angle,°	17.86 (4.46)	13.92 (2.98)	<0.001
LVES twist,°	6.19 (1.53)	4.48 (0.90)	<0.001
LVES rotation, distal,°	13.99 (4.44)	9.88 (3.22)	<0.001

Significant p value <0.05.
Abbreviations as in Table 2.

DISCUSSION

In the current study, we have described a mechanistic rationale for supranormal EF in a well-characterized HTN patient population. To this objective, we have described global and regional LV mechanics and remodeling in HTN with

Table 4. LV Geometry and Torsion (Female)

	HTN (±SD)	Control (±SD)	p Value
LVEDD, cm	4.98 (0.50)	4.84 (0.46)	NS
LVESD, cm	3.24 (0.59)	3.45 (0.41)	0.04
LVEDV, ml	121.8 (25.4)	120.1 (24.8)	NS
LVESV, ml	34.5 (16.1)	43.0 (13.1)	0.04
LVED sphericity index	1.63 (0.22)	1.79 (0.20)	0.006
LVES sphericity index	1.97 (0.38)	1.95 (0.25)	NS
LVED apex curvature, cm^{-1}	1.37 (0.32)	1.49 (0.28)	NS
LVES apex curvature, cm^{-1}	3.99 (2.42)	3.06 (1.18)	NS
LVED apex curvature index	0.32 (0.07)	0.28 (0.06)	0.04
LVES apex curvature index	0.21 (0.09)	0.22 (0.08)	NS
LV mass, g	112.28 (34.00)	82.37 (18.73)	<0.001
LV mass index 1, mass/BSA	59.77 (15.98)	45.94 (10.32)	<0.001
LV mass index 2, mass/$Ht^{2.7}$	30.79 (8.69)	20.50 (4.84)	<0.001
Mass/LVEDV, gm/ml	0.94 (0.26)	0.70 (0.15)	<0.001
LVEF, %	72 (8.8)	65 (6.3)	<0.001
LVES torsion angle,°	18.41 (4.59)	14.16 (3.11)	<0.001
LVES twist,°	6.41 (1.51)	4.63 (1.00)	<0.001
LVES rotation, distal,°	14.78 (3.51)	9.60 (3.90)	<0.001

Significant p value <0.05.
Abbreviations as in Table 2.

Table 5. Regional LV Remodeling and Wall Stress

	Base			Mid			Distal		
	HTN	Control (±SD)	p Value	HTN	Control	p Value	HTN	Control	p Value
LVED circ. curv., cm^{-1}	0.38 (0.04)	0.38 (0.03)	NS	0.40 (0.04)	0.40 (0.03)	NS	0.49 (0.06)	0.50 (0.04)	NS
LVED long. curv., cm^{-1}	0.19 (0.02)	0.19 (0.02)	NS	0.07 (0.04)	0.06 (0.03)	NS	0.20 (0.04)	0.18 (0.04)	0.021 (NS)
LVED wall thickness, cm	1.02 (0.21)	0.78 (0.14)	<0.001	0.88 (0.18)	0.69 (0.14)	<0.001	0.67 (0.14)	0.57 (0.13)	<0.001
LV wall thickening, %	58.4 (19.5)	47.0 (14.8)	0.001	78.3 (24.5)	63.8 (16.5)	<0.001	100.7 (36.1)	75.3 (27.7)	<0.001
LVED R/T ratio	2.67 (0.58)	3.47 (0.66)	<0.001	3.04 (0.73)	3.79 (0.86)	<0.001	3.26 (0.85)	3.77 (1.04)	0.005 (NS)
LVES R/T ratio	1.11 (0.30)	1.65 (0.38)	<0.001	1.09 (0.36)	1.61 (0.38)	<0.001	1.05 (0.41)	1.47 (0.41)	<0.001
LVES wall stress, 1,000 N/m^2	7.76 (2.94)	10.53 (2.57)	<0.001	7.40 (3.48)	9.83 (2.55)	<0.001	7.07 (3.86)	8.80 (2.83)	0.001

Values are mean ± SD. Significant p value <0.0024.
circ. curv. = circumferential curvature; long. curv. = longitudinal curvatures; R/T = radius of curvature to wall thickness ratio; other abbreviations as in Tables 1 and 2.

normal EF. We demonstrate that there is increased torsional deformation in the HTN group as compared with controls that is predominantly due to increased rotation of the distal/apical segments of the LV. We have also confirmed that Ell and Ecc strains are depressed at regional LV levels in the HTN group. However, we found that the principal strain representative of maximal shortening (E3) at the same corresponding levels is similar in the 2 groups. This apparent paradox may be accounted for by the change in the directions of principal components of strain tensors in the HTN group compared with controls. We also found that there is differential LV remodeling in the HTN group compared with controls that manifest, not only as an increase in LV mass and wall thickness, but also as a higher LV apical curvature index at end-diastole. Furthermore, there is reduced end-systolic LV wall stress in the HTN group. Taken together, these resulted in greater LV wall thickening and supranormal EF in HTN despite lower longitudinal and circumferential strains.

Studies in individual myofibers have shown that a 15% fiber shortening leads to only an 8% increase in myocyte diameter (i.e., individual cell thickening), which cannot by itself account for the observed >40% LV radial wall thickening and a >60% LVEF (27,28). The increased wall thickness seen in HTN with concentric remodeling has been shown to be associated with preserved EF and reduced circumferential shortening (29). Recent research using theoretical models (30,31) and validated in humans (31) has suggested that the geometric effects of increased radius to wall thickness ratio in concentric remodeling offset reductions in circumferential shortening, allowing EF to be preserved. In our HTN group, we found increased LV wall thickening at all LV levels. This increased thickening in HTN occurred despite a decrease in longitudinal and circumferential strains at various segments. Interestingly, we did not find any differences in the measurements of maximal shortening (E3) across various segments of the LV. This made us evaluate the directional vector of the strain tensors. We found that there were differences in the directional vector that may account for similar E3 in the 2 groups despite differences in Ell and Ecc. In contrast to our findings, recently investigators used 2D echocardiographic speckle tracking techniques to evaluate Ecc, Ell, and radial strains (Err) at the papillary muscle level in patients with mild HTN. They demonstrated no difference in the measurements between normal and HTN (32). However, other

Table 6. Regional LV Strains

	Base			Mid			Distal		
	HTN (±SD)	Control (±SD)	p Value	HTN (±SD)	Control (±SD)	p Value	HTN (±SD)	Control (±SD)	p Value
LVES Ecc	13.10 (2.62)	13.99 (1.87)	0.055 (NS)	14.24 (3.28)	15.81 (1.65)	0.004	13.97 (4.45)	16.69 (2.63)	<0.001
LVES Ell	10.59 (3.37)	13.16 (2.18)	<0.001	10.67 (3.45)	12.33 (2.43)	0.006	12.12 (4.66)	11.78 (3.66)	NS
LVES E3	20.01 (2.31)	19.72 (1.84)	NS	19.90 (2.56)	19.84 (1.95)	NS	22.75 (3.26)	22.59 (2.66)	NS

Significant p value <0.0056.
E3 = maximum shortening strain; Ecc = circumferential strain; Ell = longitudinal strain; other abbreviations as in Table 1.

Table 7. Angles Between Principal Strain Directions and Normal Strain (Circumferential, Longitudinal, and Radial) Directions

	Base			Mid			Distal		
	HTN (±SD)	Control (±SD)	p Value	HTN (±SD)	Control (±SD)	p Value	HTN (±SD)	Control (±SD)	p Value
Ecc angle,°	37.22 (4.03)	36.08 (3.26)	NS	33.86 (4.68)	30.68 (4.87)	<0.001	35.41 (5.08)	31.07 (5.27)	<0.001
Ell angle,°	38.49 (3.99)	37.05 (3.72)	0.06 (NS)	35.16 (4.47)	33.13 (6.20)	0.004	36.46 (6.32)	35.49 (7.42)	NS
Err angle,°	15.91 (7.79)	14.89 (7.41)	NS	16.64 (6.41)	14.97 (7.86)	NS	26.57 (11.39)	24.62 (11.22)	NS

Significant p value <0.0056.
HTN = hypertension; other abbreviations as in Tables 1 and 6.

investigators using similar techniques such as ours have demonstrated depressed circumferential strains in HTN patients as compared with the control population (33).

We noted that LV torsion was increased in HTN that predominantly was due to increased rotation at the distal segment. Our current observations are consistent with the theoretical assumption that predicts a greater torsion in the presence of increased concentricity (decreased R/T ratio) due to increased mechanical torque advantage of subepicardial fibers over subendocardial fibers (6,7,9,34). In support of this hypothesis, previous studies in patients with aortic valve stenosis and preserved LVEF reported an increase in LV torsion (35). Similarly, in a small cohort of older individuals with higher blood pressure compared with controls, the investigators found greater systolic torsion using a 3D-tagged CMR analytical technique (36). In patients with hypertrophic cardiomyopathy, torsion was increased in the presence of significantly decreased myocardial strains, which was attributed to the myofibrillar disarray of this condition (17).

Study limitations. The major limitations of our study are that there were differences in the mean age and BMI of the 2 groups. We adjusted for these variables and still found significantly higher torsion and twist in the HTN group. In a large population cohort, 1 group of researchers has demonstrated an age dependence of Ecc (37); in contrast, other investigators have found no significant effect of aging on myocardial strains (38,39). All participants in the HTN group by definition were on multiple antihypertensive medications, including beta-blockers and calcium channel blockers. These medications can affect the ventricular strains. However, the effects of drugs would not explain the discordance in maximal shortening strains (E3) compared with Ell and Ecc in the 2 groups.

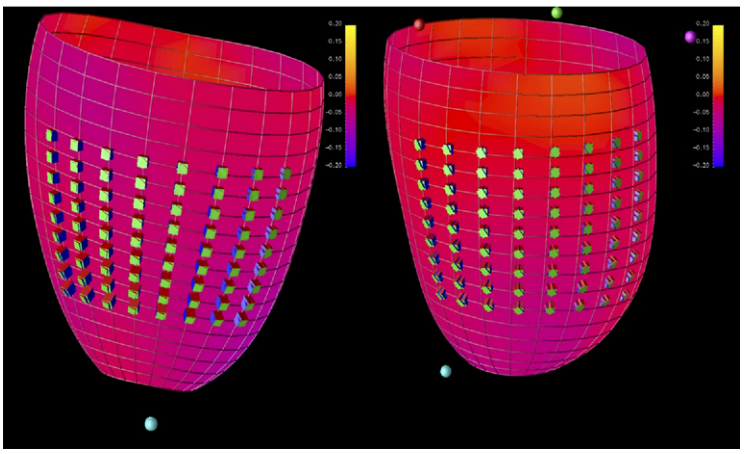

Figure 2. Representative Example of Myocardial Strains on the Lateral Wall of the LV in Control and HTN

The lateral wall of the left ventricle (LV) in normal control is shown on the **left** and in hypertension (HTN) on the **right**. Two **boxes** are shown at each point. One **box** has faces perpendicular to the radial, circumferential, and longitudinal directions. The other **box** is deformed by the principal strain tensor at that point. Please note the differences in the angles between NRM and HTN amongst the strain vectors, which are summarized in Table 7.

CONCLUSIONS

In HTN with preserved EF, we demonstrate increased LV torsion that is associated with concentric LV remodeling. Furthermore, despite depressed Ecc and Ell, LV wall thickening is increased in HTN that again is related to LV remodeling. Therefore, compensated LV remodeling is the predominant factor for supranormal EF in HTN.

Reprint requests and correspondence: Dr. Himanshu Gupta, BDB 101, CVMRI, UAB (Medicine-Cardiovascular Disease), 1530 3rd Avenue South, Birmingham, Alabama 35294-0012. *E-mail: hgupta@uab.edu.*

REFERENCES

1. Levy D, Larson MG, Vasan RS, Kannel WB, Ho KK. The progression from hypertension to congestive heart failure. JAMA 1996;275:1557–62.
2. Grossman W, Jones D, McLaurin LP. Wall stress and patterns of hypertrophy in the human left ventricle. J Clin Invest 1975;56:56–64.
3. de Simone G, Devereux RB, Roman MJ, et al. Assessment of left ventricular function by the midwall fractional shortening/end-systolic stress relation in human hypertension. J Am Coll Cardiol 1994;23:1444–51.
4. Palmon LC, Reichek N, Yeon SB, et al. Intramural myocardial shortening in hypertensive left ventricular hypertrophy with normal pump function. Circulation 1994;89:122–31.
5. Sadler DB, Aurigemma GP, Williams DW, Reda DJ, Materson BJ, Gottdiener JS. Systolic function in hypertensive men with concentric remodeling. Hypertension 1997;30:777–81.
6. Arts T, Reneman RS. Dynamics of left ventricular wall and mitral valve mechanics—a model study. J Biomech 1989;22:261–71.
7. Arts T, Reneman RS, Veenstra PC. A model of the mechanics of the left ventricle. Ann Biomed Eng 1979;7:299–318.
8. Gotte MJ, Germans T, Russel IK, et al. Myocardial strain and torsion quantified by cardiovascular magnetic resonance tissue tagging: studies in normal and impaired left ventricular function. J Am Coll Cardiol 2006;48:2002–11.
9. Lumens J, Delhaas T, Arts T, Cowan BR, Young AA. Impaired subendocardial contractile myofiber function in asymptomatic aged humans, as detected using MRI. Am J Physiol Heart Circ Physiol 2006;291:H1573–9.
10. Sallin EA. Fiber orientation and ejection fraction in the human left ventricle. Biophys J 1969;9:954–64.
11. LeGrice IJ, Takayama Y, Covell JW. Transverse shear along myocardial cleavage planes provides a mechanism for normal systolic wall thickening. Circ Res 1995;77:182–93.
12. Beyar R, Sideman S. Effect of the twisting motion on the nonuniformities of transmyocardial fiber mechanics and energy demand—a theoretical study. IEEE Trans Biomed Eng 1985;32:764–9.
13. Beyar R, Sideman S. Left ventricular mechanics related to the local distribution of oxygen demand throughout the wall. Circ Res 1986;58:664–77.
14. Zerhouni EA, Parish DM, Rogers WJ, Yang A, Shapiro EP. Human heart: tagging with MR imaging—a method for noninvasive assessment of myocardial motion. Radiology 1988;169:59–63.
15. Moore CC, Lugo-Olivieri CH, McVeigh ER, Zerhouni EA. Three-dimensional systolic strain patterns in the normal human left ventricle: characterization with tagged MR imaging. Radiology 2000;214:453–66.
16. O'Dell WG, Moore CC, Hunter WC, Zerhouni EA, McVeigh ER. Three-dimensional myocardial deformations: calculation with displacement field fitting to tagged MR images. Radiology 1995;195:829–35.
17. Young AA, Kramer CM, Ferrari VA, Axel L, Reichek N. Three-dimensional left ventricular deformation in hypertrophic cardiomyopathy. Circulation 1994;90:854–67.
18. Castillo E, Osman NF, Rosen BD, et al. Quantitative assessment of regional myocardial function with MR-tagging in a multi-center study: interobserver and intraobserver agreement of fast strain analysis with Harmonic Phase (HARP) MRI. J Cardiovasc Magn Reson 2005;7:783–91.
19. Young AA, Orr R, Smaill BH, Dell'Italia LJ. Three-dimensional changes in left and right ventricular geometry in chronic mitral regurgitation. Am J Physiol 1996;271 Pt 2:H2689–700.
20. Lipshultz M. Differential Geometry. New York, NY: McGraw-Hill, 1969.
21. Cerqueira MD, Weissman NJ, Dilsizian V, et al. Standardized myocardial segmentation and nomenclature for tomographic imaging of the heart: a statement for healthcare professionals from the Cardiac Imaging Committee of the Council on Clinical Cardiology of the American Heart Association. Circulation 2002;105:539–42.
22. Di Donato M, Dabic P, Castelvecchio S, et al., for the RESTORE Group. Left ventricular geometry in normal and post-anterior myocardial infarction patients: sphericity index and 'new' conicity index comparisons. Eur J Cardiothorac Surg 2006;29 Suppl 1:S225–30.
23. Denney TS Jr., Gerber BL, Yan L. Unsupervised reconstruction of a three-dimensional left ventricular strain from parallel tagged cardiac images. Magn Reson Med 2003;49:743–54.
24. Li J, Denney TS Jr. Left ventricular motion reconstruction with a prolate spheroidal B-spline model. Phys Med Biol 2006;51:517–37.
25. Aelen FWL, Arts T, Sanders DGM, et al. Relation between torsion and cross-sectional area change in the human left ventricle. J Biomech 1997;30:207–12.
26. Rüssel I, Götte M, Bronzwaer J, Knaapen P, Paulus W, van Rossum AC. Left ventricular torsion: an expanding role in the analysis of myocardial dysfunction. J Am Coll Cardiol Img 2009;2:648–55.
27. Rademakers FE, Rogers WJ, Guier WH, et al. Relation of regional cross-fiber shortening to wall thickening in the intact heart. Three-dimensional strain analysis by NMR tagging. Circulation 1994;89:1174–82.
28. Spann JF Jr., Buccino RA, Sonnenblick EH, Braunwald E. Contractile state of cardiac muscle obtained from cats with experimentally produced ventricular hypertrophy and heart failure. Circ Res 1967;21:341–54.
29. Aurigemma GP, Silver KH, Priest MA, Gaasch WH. Geometric changes allow normal ejection fraction despite depressed myocardial shortening in hypertensive left ventricular hypertrophy. J Am Coll Cardiol 1995;26:195–202.

30. Vandsburger MH, French BA, Helm PA, et al. Multi-parameter in vivo cardiac magnetic resonance imaging demonstrates normal perfusion reserve despite severely attenuated Î²-adrenergic functional response in neuronal nitric oxide synthase knockout mice. Eur Heart J 2007;28:2792–8.
31. Zha W, Lloyd SG, Gupta H, Dell'Italia LJ, Denney TSJ. Preserved ejection fraction in the presence of reduced LV wall strain in hypertension: a geometric explanation validated by MRI. Proceedings of the 19th Scientific Meeting of ISMRM; May 7–13, 2011; Montréal, Québec, Canada.
32. Narayanan A, Aurigemma GP, Chinali M, Hill JC, Meyer TE, Tighe DA. Cardiac mechanics in mild hypertensive heart disease: a speckle-strain imaging study. Circ Cardiovasc Imaging 2009;2:382–90.
33. Biederman RWW, Doyle M, Young AA, et al. Marked regional left ventricular heterogeneity in hypertensive left ventricular hypertrophy patients: a Losartan Intervention for Endpoint Reduction in Hypertension (LIFE) cardiovascular magnetic resonance and echocardiographic substudy. Hypertension 2008;52:279–86.
34. Van der Toorn A, Barenbrug P, Snoep G, et al. Transmural gradients of cardiac myofiber shortening in aortic valve stenosis patients using MRI tagging. Am J Physiol Heart Circ Physiol 2002;283:H1609–15.
35. Stuber M, Scheidegger MB, Fischer SE, et al. Alterations in the local myocardial motion pattern in patients suffering from pressure overload due to aortic stenosis. Circulation 1999; 100:361–8.
36. Fonseca CG, Oxenham HC, Cowan BR, Occleshaw CJ, Young AA. Aging alters patterns of regional nonuniformity in LV strain relaxation: a 3-D MR tissue tagging study. Am J Physiol Heart Circ Physiol 2003;285: H621–30.
37. Cheng S, Fernandes VRS, Bluemke DA, McClelland RL, Kronmal RA, Lima JAC. Age-related left ventricular remodeling and associated risk for cardiovascular outcomes: the Multi-Ethnic Study of Atherosclerosis. Circ Cardiovasc Imaging 2009;2:191–8.
38. Marwick TH, Leano RL, Brown J, et al. Myocardial strain measurement with 2-dimensional speckle-tracking echocardiography: definition of normal range. J Am Coll Cardiol Img 2009;2:80–4.
39. Sun JP, Popovic ZB, Greenberg NL, et al. Noninvasive quantification of regional myocardial function using Doppler-derived velocity, displacement, strain rate, and strain in healthy volunteers: effects of aging. J Am Soc Echocardiogr 2004;17:132–8.

Key Words: hypertension ■ left ventricular hypertrophy ■ strain ■ torsion.